This is the accepted manuscript made available via CHORUS. The article has been published as:

Optimized cavity-mediated dispersive two-qubit gates between spin qubits

M. Benito, J. R. Petta, and Guido Burkard

Phys. Rev. B **100**, 081412 — Published 29 August 2019

DOI: 10.1103/PhysRevB.100.081412

Optimized cavity-mediated dispersive two-qubit gates between spin qubits

M. Benito,[1] J. R. Petta,[2] and Guido Burkard[1]

[1] *Department of Physics, University of Konstanz, D-78457 Konstanz, Germany*
[2] *Department of Physics, Princeton University, Princeton, New Jersey 08544, USA*

The recent realization of a coherent interface between a single electron in a silicon quantum dot and a single photon trapped in a superconducting cavity opens the way for implementing photon-mediated two-qubit entangling gates. In order to couple a spin to the cavity electric field some type of spin-charge hybridization is needed, which impacts spin control and coherence. In this work we propose a cavity-mediated two-qubit gate and calculate cavity-mediated entangling gate fidelities in the dispersive regime, accounting for errors due to the spin-charge hybridization, as well as photon- and phonon-induced decays. By optimizing the degree of spin-charge hybridization, we show that two-qubit gates mediated by cavity photons are capable of reaching fidelities exceeding 90% in present-day device architectures. High iSWAP gate fidelities are achievable even in the presence of charge noise at the level of $2\,\mu$eV.

Introduction. Recent advances in semiconductor fabrication, manipulation and readout techniques have situated spin qubits among the most promising candidates for quantum information processing [1–3]. The degree of control over single-electron spin qubits and their exchange interaction has allowed high fidelity single [4–6] and two-qubit [7–11] gates. Moreover, recent improvements in the fabrication of semiconductor quantum dots (QDs) has pushed the limits of QD modules to sizable linear [12, 13] and two-dimensional [14, 15] arrays, which could allow not only the implementation of multielectron encoded qubits but also intra-module operations and electron transfer [16]. Several proposals exist to create a modular quantum architecture [17, 18] with all-to-all connectivity, which permits universal distributed quantum computation and high tolerances in error-correcting codes [19].

Within the approach of circuit quantum electrodynamics (QED) [20–25], the microwave field of a superconducting transmission line resonator (cavity) mediates interactions between qubits separated by macroscopic distances, allowing a fully scalable and modular quantum information processing device [26]. Although electron spin qubits in semiconductor QDs promise long coherence times and potential for scalability, these photon-mediated interactions have not yet been demonstrated for spin qubits. It is precisely the interesting coherent behavior of the electron spin with its small magnetic dipole moment that makes it difficult to couple distant spins via a cavity.

In this paper, we show how this problem can be overcome by introducing an optimized spin-charge hybridization of each qubit. Recent experiments showing strong spin-cavity coupling [27–30] have given up part of the spin qubit coherence to gain in electric dipole coupling by hybridizing the spin and charge degrees of freedom. To extend this idea to cavity-mediated coupling, we focus on the single-electron qubit [31] in a double quantum dot (DQD), where the mixing of orbital motion and spin is induced by an externally imposed magnetic field gradient, and show that the spin qubit outperforms the intrinsic charge qubit both in the resonant and dispersive regime for levels of decoherence encountered in state-of-the-art devices.

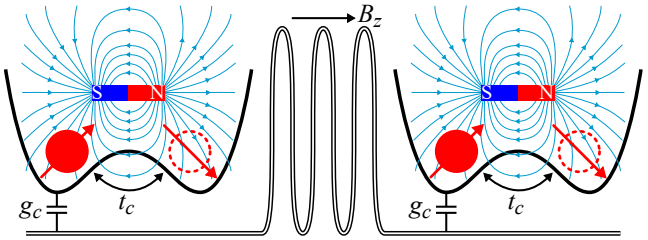

Figure 1. Schematic illustration of two DQDs capacitively coupled to the same microwave superconducting resonator (cavity). The electrons tunnel between the two respective QDs with tunnel coupling t_c, forming charge qubits which are transversely coupled to the cavity with strength g_c. The electron spin is influenced by a homogeneous external magnetic field B_z and the transverse field gradient induced by the micromagnet.

Although the spin-photon coupling strength is only a fraction of the charge-photon coupling [27, 28], the spin decoherence is much slower and can be made comparable to the cavity loss rate, which allows for strong spin-photon coupling [32, 33]. In the dispersive regime the qubit and photon frequencies are detuned and we find that the externally-controllable spin-charge hybridization allows for optimal detuning values implying high-fidelity two-qubit gates. The dispersive coupling scheme demands a relatively small degree of spin-charge hybridization and will benefit enormously from the use of isotopically purified ^{28}Si material [4, 6, 34, 35].

Model. We consider two DQDs capacitively coupled to the same cavity mode with frequency ω_c (Fig. 1). Both DQDs are electrically tuned into the symmetric single-electron regime, with the electronic charge distributed between the two QDs. The tunnel coupling t_c and energy level detuning ϵ can be electrically controlled. The electron is capacitively coupled to the cavity electric

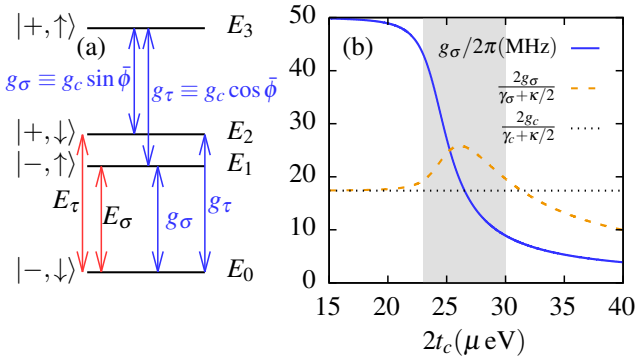

Figure 2. (a) Energy levels, $|\pm,\uparrow(\downarrow)\rangle = |\pm\rangle \otimes |\uparrow(\downarrow)\rangle$, with $\tau_z|\pm\rangle = \pm|\pm\rangle$ and $\sigma_z|\uparrow(\downarrow)\rangle = \pm|\uparrow(\downarrow)\rangle$, for an electron localized in a DQD under the influence of an inhomogeneous magnetic field. The energy difference (red arrow) between ground and first (second) excited states is E_σ (E_τ). Blue arrows represent coherent coupling via cavity photons, with coupling strengths g_σ and g_τ. (b) Coupling strength g_σ (solid blue line) as a function of the tunnel splitting $2t_c$ for a fixed magnetic field profile; $B_z = 24\,\mu$eV and $b_x = 2\,\mu$eV. Also shown are the ratio between the coupling and decoherence for the spin (dashed orange line) and charge (dotted black line) qubit, for $g_c/2\pi = 50$ MHz, $\gamma_c/2\pi = 5$ MHz, and $\kappa/2\pi = 1.5$ MHz. The shaded area indicates the regime where the spin qubit outperforms the charge qubit.

field [22, 36–39]. An externally applied global magnetic field B_z Zeeman splits the spin states and magnetizes the micromagnets located near the DQDs. The longitudinal component of the micromagnet field adds to B_z and the micromagnet generates a transverse field gradient b_x (typically $\lesssim 1\,$mT/nm). A single DQD can be described with a model Hamiltonian $\tilde{H} = \tilde{H}_0 + \tilde{H}_I$ with $\tilde{H}_0 = t_c\tilde{\tau}_x + \epsilon\tilde{\tau}_z/2 + B_z\tilde{\sigma}_z/2 + b_x\tilde{\sigma}_x\tilde{\tau}_z/2 + \omega_c a^\dagger a$, where $\tilde{\tau}_k$ and $\tilde{\sigma}_k$, for $k = x, y, z$, are the position and spin Pauli matrices, respectively, and $a, a^\dagger$ are the cavity photon operators. In the following, we will study a symmetric DQD with $\epsilon = 0$, unless noted otherwise. Here $\hbar = 1$ and magnetic fields are given in energy units. The light-matter interaction is described by $\tilde{H}_I = g_c\tilde{\tau}_z(a + a^\dagger)$, where g_c is the electric dipole coupling strength between the DQD electron and a cavity photon. Due to the spin-orbit effect induced by b_x, the electron spin dynamics are sensitive to the cavity electric field [32, 33, 40, 41].

In the following we work in the basis that diagonalizes $\tilde{H}_0$, where bonding and antibonding states of the DQD with opposite spin are hybridized [33]. Using new Pauli matrices τ_k, σ_k leads to the transformed Hamiltonians $H_0 = E_\tau\tau_z/2 + E_\sigma\sigma_z/2 + \omega_c a^\dagger a$ and

$$H_I = (-g_\tau\tau_x + g_\sigma\sigma_x\tau_z)(a + a^\dagger)\,, \qquad (1)$$

with the energy levels at $E_{\tau(\sigma)} = E_{2(1)} - E_0$, where $E_{3(2)} = -E_{0(1)} = \sqrt{(2t_c \pm B_z)^2 + b_x^2}/2$, coupled to the cavity with strength $g_\tau = g_c\cos\bar{\phi}$ and $g_\sigma = g_c\sin\bar{\phi}$, where $\bar{\phi} = (\phi_+ + \phi_-)/2$ is the spin-charge mixing angle, with $\phi_\pm = \arctan[b_x/(2t_c \pm B_z)]$. The corresponding level scheme is shown in Fig. 2(a). In Fig. 2(b) we show how the coupling strength g_σ decreases with increasing tunnel coupling t_c for a given magnetic field profile, as a consequence of the increasing spin character of the qubit. If the qubit energy E_σ equals the photon frequency ω_c, coherent state transfer between a cavity photon and the qubit is possible whenever g_σ overcomes the total decoherence rate $\gamma_\sigma + \kappa/2$, where κ is the cavity loss rate. Typical cavity photon frequencies are around $\omega_c \sim 2\pi\,6\,\text{GHz} \sim 25\,\mu$eV. In Fig. 2(b), we show the ratio between coupling and decoherence for the system with (dashed line) and without (dotted line) magnetic fields, i.e., for a spin and a charge qubit respectively, assuming that the decoherence rate of the former is inherited from the hybridization with charge, $\gamma_\sigma = \gamma_c\sin^2\bar{\phi}$, where γ_c is the total charge decoherence rate. Although the charge qubit can be made sufficiently coherent to reach the strong coupling regime [38, 39, 42], the spin qubit overcomes its performance in the shaded gray area in Fig. 2(b) ($2t_c \gtrsim B_z$) if $\gamma_c > \kappa/2$. More precisely, we find that the spin qubit performs better than the charge qubit when $\sin\bar{\phi} > \kappa/2\gamma_c$ in a finite interval around $2t_c \approx B_z$. In this regime, the gain from using the spin with a long coherence time overcompensates the decrease in coherence from spin-charge hybridization. Therefore, the advantage to be gained from using spin rather than charge as a qubit is twofold: (i) In the regime indicated by the shaded region in Fig. 2(b), the exchange of quantum information between the qubit and the cavity photons is more efficient for the spin, and (ii) the spin-charge and spin-photon couplings can be switched off efficiently by controlling t_c and the level detuning ϵ, thus reaching a memory qubit regime where the spin qubit is far more coherent than the charge qubit. Importantly, in order to control the interaction times, there are two mechanisms to electrically switch off g_σ: a) increasing t_c (Fig. 2), or b) increasing ϵ and thereby reducing the charge admixture across the DQD, such that the charge-photon coupling is reduced to $\tilde{g}_c = 2t_c g_c/\sqrt{\epsilon^2 + 4t_c^2}$.

When two DQDs as described above are coupled to the same cavity, the cavity photons can induce a long-distance coupling between their spins. In the resonant regime ($E_\sigma = \omega_c$) a collectively-enhanced two-qubit coupling can be observed in a transmission experiment [42–44]. Here we investigate the dispersive regime, where the photon and qubit frequencies are detuned and a coherent long-distant interaction is mediated by the exchange of virtual photons [20, 45, 46], resulting in a smaller effective coupling which is less sensitive to photon loss in the cavity.

Dispersive regime. The light-matter interaction Hamiltonian (1) couples subspaces with different photon numbers. For small coupling strengths $g_{\tau(\sigma)} \ll |E_{\tau(\sigma)} - \omega_c|$, we can decouple such subspaces to a desired order using a Schrieffer-Wolff transformation [47]. From now

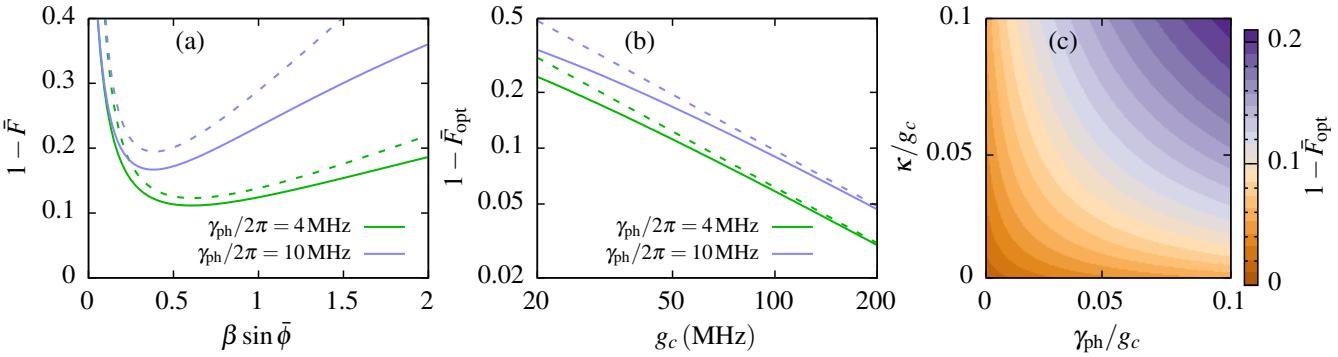

Figure 3. (a) Average infidelity of an iSWAP gate between spin qubits as a function of $\beta\sin\bar{\phi}$, where $\beta = \Delta/g_\sigma$ is the qubit-photon detuning in units of the spin-photon coupling, and $\bar{\phi}$ is the spin-charge mixing angle, for the indicated values of $\gamma_{\rm ph}$. Here, we have chosen the charge coupling strength $g_c/2\pi = 50\,$MHz. (b) Double-logarithmic plot of the optimal average infidelity $1-\bar{F}_{\rm opt}$ as a function of g_c for the same values of $\gamma_{\rm ph}$. In (a) and (b) the photon loss rate is $\kappa/2\pi = 1.5\,$MHz and the solid lines correspond to Eq. (4) while the dashed lines correspond to the approximated result in Eq. (5). (c) Optimal average infidelity $1-\bar{F}_{\rm opt}$ as a function of $\gamma_{\rm ph}/g_c$ and κ/g_c.

on we assume $2t_c > B_z$, which ensures that the lower-energy subspace constitutes a qubit with a good coherence inherited from its spin character. Therefore the most interesting operating regime is the one with the cavity frequency ω_c being close to E_σ, fulfilling the condition, $g_\tau|\Delta|/|E_\tau - \omega_c| \ll g_\sigma \ll |\Delta|$, with the detuning $\Delta = E_\sigma - \omega_c$.

Assuming identical DQDs ($i = 1, 2$), we find to first order in the perturbative parameter g_σ/Δ, in the limit of an empty cavity and within a rotating-wave approximation (RWA) [47], the dispersive Hamiltonian in the rotating frame

$$\tilde{H}^{\rm d} \simeq \frac{g_\sigma^2}{\Delta}\left(\sigma_+^{(1)}\sigma_-^{(2)} + \sigma_-^{(1)}\sigma_+^{(2)}\right)\tau_z^{(1)}\tau_z^{(2)}. \tag{2}$$

The goal now is to harness the spin-spin long-distance coupling to perform a two-qubit gate. A coupling of the form $\sim g_\sigma^2\left(\sigma_+^{(1)}\sigma_-^{(2)} + h.c.\right)/\Delta$ performs an iSWAP gate at gate times $t_g = (4m+1)\frac{\pi}{2}\frac{|\Delta|}{g_\sigma^2}$ for any integer m, e.g. $|\uparrow,\downarrow\rangle \to i\,|\downarrow,\uparrow\rangle$. A CNOT entangling gate can be constructed with two iSWAP gates and single qubit rotations [45, 48]. To estimate the performance of such a gate we take into account three error sources: (1) cavity-mediated long-distance τ-coupling, and $\sigma^{(i)}$-$\tau^{(i)}$ coupling within a DQD as well as between distant DQDs ($\sigma^{(1)}$-$\tau^{(2)}$) [47]; (2) spin-charge hybridization making the spin qubits susceptible to charge noise due to electron-phonon interaction and other charge fluctuations commonly present in semiconductor nano-structures; (3) cavity damping due to dressing of spin qubits by photonic excitations.

To capture dissipative effects, we model the system consisting of two DQDs using a quantum master equation (QME) in the dispersive regime [49]. Assuming that the system is prepared in the lower energy charge sector, we derive an effective QME for the reduced spin density matrix $\rho_\sigma^{\rm d}$,

$$\dot{\tilde{\rho}}_\sigma^{\rm d} \simeq \frac{-ig_\sigma^2}{\Delta}\left[\sigma_+^{(1)}\sigma_-^{(2)} + h.c., \tilde{\rho}_\sigma^{\rm d}\right] + \frac{\kappa g_\sigma^2}{2\Delta^2}\mathcal{D}\left[\sigma_-^{(1)} + \sigma_-^{(2)}\right]\tilde{\rho}_\sigma^{\rm d} + \frac{\gamma_{\rm ph}}{2}\sin^2\bar{\phi}\left(\mathcal{D}\left[\sigma_-^{(1)}\right] + \mathcal{D}\left[\sigma_-^{(2)}\right]\right)\tilde{\rho}_\sigma^{\rm d}\,, \tag{3}$$

where $\mathcal{D}[c]$ represents the Lindblad superoperator $\mathcal{D}[c]\,\rho = 2c\rho c^\dagger - c^\dagger c\rho - \rho c^\dagger c$. The first term in Eq. (3) describes the cavity-mediated long-distance coupling, with strength g_σ^2/Δ, while the second term describes Purcell relaxation with rate $\kappa g_\sigma^2/\Delta^2$. The last term describes relaxation due to phonon emission with rate $\gamma_{\rm ph}$ (at the qubit energy E_σ) in each DQD. Given the reported long electron spin coherence times in silicon QDs, we neglect other decoherence sources such as hyperfine interaction with nuclear spins [2].

Results. Using our effective model describing the system dynamics, we now estimate how accurately one can expect to realize a two-spin-qubit iSWAP gate taking into account the amount of decoherence encountered in present-day experiments. We determine the quality of the quantum gate via the average fidelity $\bar{F}$, which compares the targeted pure state and the obtained mixed state density matrix, averaged over all possible pure input states [50–54].

Choosing a spin qubit-cavity detuning $|\Delta| = \beta g_\sigma$ with $\beta \gg 1$ to ensure the dispersive regime and a gate time corresponding to the shortest iSWAP gate, $t_g = \pi\beta/(2g_\sigma)$, we find for Eq. (3)

$$\bar{F} = \frac{1}{20}\left[4 + (1+x)^2(1+xy)^2\right] \tag{4}$$

with $x = e^{-\pi\gamma_{\rm ph}\beta\sin\bar{\phi}/(4g_c)}$ and $y = e^{-\pi\kappa/(2\beta\sin\bar{\phi}g_c)}$, which for $\gamma_{\rm ph}\beta\sin\bar{\phi}, \kappa/(\beta\sin\bar{\phi}) \ll g_c$ can be approximated as

$$\bar{F} \simeq 1 - \frac{2\pi}{5g_c}\left(\gamma_{\rm ph}\beta\sin\bar{\phi} + \frac{\kappa}{\beta\sin\bar{\phi}}\right)\,. \tag{5}$$

This approximated result suggests an optimal value of $\beta \sin\bar{\phi}$, related to the detuning Δ, that maximizes $\bar{F}$,

$$(\beta \sin\bar{\phi})_{\rm opt} \simeq \sqrt{\frac{\kappa}{\gamma_{\rm ph}}} \ , \tag{6}$$

with a corresponding approximated average fidelity of

$$\bar{F}_{\rm opt} \simeq 1 - \frac{4\pi}{5}\sqrt{\frac{\gamma_{\rm ph}\kappa}{g_c^2}} \ . \tag{7}$$

Although $\bar{F}_{\rm opt}$ is determined by charge qubit and cavity parameters, via the cooperativity $C = g_c^2/\gamma_{\rm ph}\kappa$, the role of the spin-charge hybridization is to enable the optimization in Eq. (6), which is not accessible for charge qubits ($\bar{\phi} = \pi/2$) unless $\gamma_{\rm ph} \ll \kappa$ (because $\beta \gg 1$).

In Fig. 3(a), we show the exact $\bar{F}$, Eq. (4), compared with the approximation, Eq. (5), as a function of $\beta \sin\bar{\phi}$ for a typical value of $g_c/2\pi = 50\,$MHz for different values of $\gamma_{\rm ph}$. The best gate can be performed at the minimum of these curves, which can be found numerically for the exact expression by demanding $\partial\bar{F}/\partial(\beta\sin\bar{\phi}) = 0$. For currently available system parameters g_c, $\gamma_{\rm ph}$, and κ, we find $\bar{F} \approx 90\%$.

Improvements are possible via all three parameters. For example, typical values of $g_c/2\pi$ are $\approx 50\,$MHz [27], but can be increased beyond 100 MHz using high kinetic inductance resonators [55, 56] or non-linear effects [57], leading to $\bar{F} \approx 95\%$. In Fig. 3(b) we show the predicted $\bar{F}_{\rm opt}$ as a function of g_c. As expected, the exact result coincides with the approximation, Eq. (7), for large g_c and $1 - \bar{F}_{\rm opt} \propto 1/g_c$. In Fig. 3(c) we show the exact $\bar{F}_{\rm opt}$ as a function of both $\gamma_{\rm ph}/g_c$ and κ/g_c. An even higher fidelity of $\bar{F} \approx 99\%$ could be reached if e.g. $g_c/2\pi \approx 100\,$MHz and $\kappa/2\pi \approx 0.01\gamma_c/2\pi \approx 0.04\,$MHz or $\kappa/2\pi \approx \gamma_c/2\pi \approx 0.4\,$MHz. Reducing κ is not a fundamental problem if one uses separate readout resonators. Working at lower magnetic fields would reduce the phonon relaxation rate [58], which could potentially be further suppressed by using phononic crystals [59, 60].

In current experiments, the magnetic field gradient b_x and the cavity frequency ω_c are fixed, but it is possible to modify the spin-charge hybridization by electrically tuning the tunnel coupling t_c. Therefore, one can tune t_c and B_z such that the optimal fidelity condition is fulfilled and the spin qubits are in the dispersive regime, $g_\sigma \ll |\Delta|$. In Fig. 4(a) (solid line), we show the average infidelity $1 - \bar{F}$ of the dispersive iSWAP gate as a function of t_c. The result for different values of b_x, g_c and the comparison with the full QME can be found in [47].

In Fig. 4(b) we illustrate a protocol to perform the two-qubit gate via time-dependent control of t_c in the two DQDs from a large value where the interactions are very weak to the optimal point and back. In Fig. 4(c), we show the energy levels, whose splittings determine how high the ramp speed v can be. To avoid cavity population and perform the described gate, v needs to lie in the regime

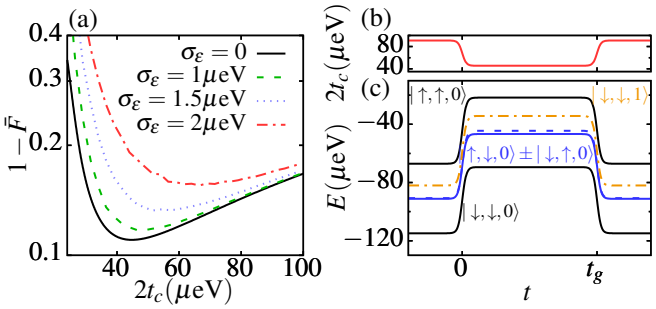

Figure 4. (a) Average infidelity of an iSWAP gate between spin qubits as a function of $2t_c$, with $b_x = 2\,\mu$eV and $\omega_c = 24\,\mu$eV in the dispersive regime, $\Delta = -10\,g_\sigma$. The charge-photon coupling is $g_c/2\pi = 50\,$MHz, the phonon relaxation rate is $\gamma_{\rm ph}/2\pi = 4\,$MHz and the cavity loss rate is $\kappa/2\pi = 1.5\,$MHz. The solid line corresponds to Eq. (4) while the other lines correspond to the indicated strength of low-frequency charge noise σ_ϵ. (b) Control of $2t_c$ as a function of time in a possible protocol to realize the gate and (c) corresponding energy levels, labeled $|\sigma_1, \sigma_2, n\rangle$, where σ_i denotes the spin qubit state in DQD i and n the number of cavity photons. The splittings given by the long-distance spin-spin interaction and the spin qubit-cavity detuning, have been exaggerated for better visibility.

$|E_\sigma - \omega_c| \gg v \gg g_\sigma^2/\Delta$, which, for typical parameters implies $v \approx 5 - 20\,$MHz.

Charge noise. The realistic entangling gates fidelities between spin qubits are currently limited by charge noise. Since in our setup the qubits are at the "sweet spot" $\epsilon = 0$, i.e., first-order insensitive to fluctuations in ϵ (with amplitude δ_i), the noise enters solely in second order. The high-frequency charge noise adds dephasing Lindblad terms to the QME (3),

$$\mathcal{L}_\phi \rho_\sigma^d = \frac{\gamma_\phi}{4}\sin^2\bar{\phi}\left(\mathcal{D}\left[\sigma_z^{(1)}\right] + \mathcal{D}\left[\sigma_z^{(2)}\right]\right)\rho_\sigma^d \ , \tag{8}$$

and the low-frequency (quasistatic) component randomizes the spin qubit energies via the Hamiltonian term

$$H_\delta = \frac{\delta_1^2 \sin^2\bar{\phi}}{4E_\sigma}\sigma_z^{(1)} + \frac{\delta_2^2\sin^2\bar{\phi}}{4E_\sigma}\sigma_z^{(2)} \ . \tag{9}$$

Accounting for high-frequency charge noise, the approximated result in Eq. (5) needs to be revised as $\gamma_{\rm ph} \to \gamma_{\rm ph} + \gamma_\phi$. To calculate the effect of the low-frequency noise, we average the fidelity over a Gaussian distribution with standard deviation σ_ϵ for δ_i, with typical values $\sigma_\epsilon \sim 1 - 4\,\mu$eV [61, 62]. The mean value of Eq. (9) only shifts the spin qubit energies and is included into the rotating frame transformation. In Fig. 4(a), we show the average infidelity $1 - \bar{F}$ of the dispersive iSWAP gate as a function of t_c for different levels σ_ϵ of low-frequency charge noise.

Conclusions. We have analyzed the performance of single-electron spin qubits in DQDs with respect to dispersive long-distance two-qubit gates mediated by virtual

cavity photons. By solving a QME, we show that this implementation benefits from the spin-charge hybridization since it allows us to optimize the average iSWAP gate fidelity $\bar{F}$, even for the decoherence rates found in state-of-the-art experiments, where the charge qubit decoherence is worse than the photon decoherence. We predict the degree of spin-charge hybridization, controlled via t_c (Fig. 4), needed to optimize iSWAP, $\beta \sin\bar{\phi} \simeq \sqrt{\kappa/\gamma_{\rm ph}}$, and explain how the spin qubit outperforms the DQD charge qubit.

The analyzed setup is capable of reaching iSWAP gate fidelities $> 90\%$ with present-day devices and can realistically reach 99%. We expect that the same analysis can be readily applied to the triple QD spin-qubit strongly coupled to a resonator [29]. The performance of other two-qubit gates [63–65] and other qubit-resonator coupling schemes, such as longitudinal coupling [54, 66, 67], will be the subject of future studies.

Note added. While finalizing this work, we became aware of a recent related study [68] where the transitions to excited states due to the influence of non-adiabatic effects during a cavity-mediated two-qubit gate in the dissipationless (unitary) case were studied.

Acknowledgments.— This work has been supported by the Army Research Office grant W911NF-15-1-0149.

[1] R. Hanson, L. P. Kouwenhoven, J. R. Petta, S. Tarucha, and L. M. K. Vandersypen, Rev. Mod. Phys. **79**, 1217 (2007).

[2] C. Kloeffel and D. Loss, Annu. Rev. Condens. Matter Phys. **4**, 51 (2013).

[3] D. D. Awschalom, L. C. Bassett, A. S. Dzurak, E. L. Hu, and J. R. Petta, Science **339**, 1174 (2013).

[4] M. Veldhorst, J. C. C. Hwang, C. H. Yang, A. W. Leenstra, B. de Ronde, J. P. Dehollain, J. T. Muhonen, F. E. Hudson, K. M. Itoh, A. Morello, and A. S. Dzurak, Nat. Nanotechnol. **9**, 981 (2014).

[5] K. Takeda, J. Kamioka, T. Otsuka, J. Yoneda, T. Nakajima, M. R. Delbecq, S. Amaha, G. Allison, T. Kodera, S. Oda, and S. Tarucha, Sci. Adv. **2**, e1600694 (2016).

[6] J. Yoneda, K. Takeda, T. Otsuka, T. Nakajima, M. R. Delbecq, G. Allison, T. Honda, T. Kodera, S. Oda, Y. Hoshi, N. Usami, K. M. Itoh, and S. Tarucha, Nat. Nanotechnol. **13**, 102 (2018).

[7] M. Veldhorst, C. H. Yang, J. C. C. Hwang, W. Huang, J. P. Dehollain, J. T. Muhonen, S. Simmons, A. Laucht, F. E. Hudson, K. M. Itoh, A. Morello, and A. S. Dzurak, Nature **526**, 410 (2015).

[8] D. M. Zajac, A. J. Sigillito, M. Russ, F. Borjans, J. M. Taylor, G. Burkard, and J. R. Petta, Science **359**, 439 (2018).

[9] T. F. Watson, S. G. J. Philips, D. R. Kawakami, E. Ward, P. Scarlino, M. Veldhorst, D. E. Savage, M. G. Lagally, M. Friesen, S. N. Coppersmith, M. A. Eriksson, and L. M. K. Vandersypen, Nature **555**, 633 (2018).

[10] W. Huang, C. H. Yang, K. W. Chan, T. Tanttu, B. Hensen, R. C. C. Leon, M. A. Fogarty, J. C. C. Hwang, F. E. Hudson, K. M. Itoh, A. Morello, A. Laucht, and A. S. Dzurak, Nature **569**, 532 (2019).

[11] X. Xue, T. F. Watson, J. Helsen, D. R. Ward, D. E. Savage, M. G. Lagally, S. N. Coppersmith, M. A. Eriksson, S. Wehner, and L. M. K. Vandersypen, Phys. Rev. X **9**, 021011 (2019).

[12] D. M. Zajac, T. M. Hazard, X. Mi, E. Nielsen, and J. R. Petta, Phys. Rev. Applied **6**, 054013 (2016).

[13] C. Volk, A. M. J. Zwerver, U. Mukhopadhyay, P. T. Eendebak, C. J. van Diepen, J. P. Dehollain, T. Hensgens, T. Fujita, C. Reichl, W. Wegscheider, and L. M. K. Vandersypen, npj Quantum Inf. **5**, 29 (2019).

[14] U. Mukhopadhyay, J. P. Dehollain, C. Reichl, W. Wegscheider, and L. M. K. Vandersypen, Appl. Phys. Lett. **112**, 183505 (2018).

[15] P.-A. Mortemousque, E. Chanrion, B. Jadot, H. Flentje, A. Ludwig, A. D. Wieck, M. Urdampilleta, C. Bauerle, and T. Meunier, arXiv:1808.06180.

[16] A. R. Mills, D. M. Zajac, M. J. Gullans, F. J. Schupp, T. M. Hazard, and J. R. Petta, Nat. Commun. **10**, 1063 (2019).

[17] J. M. Taylor, H.-A. Engel, W. Dur, A. Yacoby, C. M. Marcus, P. Zoller, and M. D. Lukin, Nat. Phys. **1**, 177 (2005).

[18] H. J. Kimble, Nature **453**, 1023 (2008).

[19] J. Preskill, Proc. R. Soc. A **454**, 385 (1998).

[20] A. Blais, R.-S. Huang, A. Wallraff, S. M. Girvin, and R. J. Schoelkopf, Phys. Rev. A **69**, 062320 (2004).

[21] A. Wallraff, D. I. Schuster, A. Blais, L. Frunzio, R.-S. Huang, J. Majer, S. Kumar, S. M. Girvin, and R. J. Schoelkopf, Nature **431**, 162 (2004).

[22] L. Childress, A. S. Sørensen, and M. D. Lukin, Phys. Rev. A **69**, 042302 (2004).

[23] A. Cottet, M. C. Dartiailh, M. M. Desjardins, T. Cubaynes, L. C. Contamin, M. Delbecq, J. J. Viennot, L. E. Bruhat, B. Douçot, and T. Kontos, J. Phys. Condens. Matter **29**, 433002 (2017).

[24] M. R. Delbecq, V. Schmitt, F. D. Parmentier, N. Roch, J. J. Viennot, G. Fève, B. Huard, C. Mora, A. Cottet, and T. Kontos, Phys. Rev. Lett. **107**, 256804 (2011).

[25] X. Gu, A. F. Kockum, A. Miranowicz, Y. xi Liu, and F. Nori, Physics Reports **718**, 1 (2017).

[26] L. DiCarlo, J. M. Chow, J. M. Gambetta, L. S. Bishop, B. R. Johnson, D. I. Schuster, J. Majer, A. Blais, L. Frunzio, S. M. Girvin, and R. J. Schoelkopf, Nature **460**, 240 (2009).

[27] X. Mi, M. Benito, S. Putz, D. M. Zajac, J. M. Taylor, G. Burkard, and J. R. Petta, Nature **555**, 599 (2018).

[28] N. Samkharadze, G. Zheng, N. Kalhor, D. Brousse, A. Sammak, U. C. Mendes, A. Blais, G. Scappucci, and L. M. K. Vandersypen, Science **359**, 1123 (2018).

[29] A. J. Landig, J. V. Koski, P. Scarlino, U. C. Mendes, A. Blais, C. Reichl, W. Wegscheider, A. Wallraff, K. Ensslin, and T. Ihn, Nature **560**, 179 (2018).

[30] T. Cubaynes, M. R. Delbecq, M. C. Dartiailh, R. Assouly, M. M. Desjardins, L. C. Contamin, L. E. Bruhat, Z. Leghtas, F. Mallet, A. Cottet, and T. Kontos, arXiv:1903.05229.

[31] D. Loss and D. P. DiVincenzo, Phys. Rev. A **57**, 120 (1998).

[32] F. Beaudoin, D. Lachance-Quirion, W. A. Coish, and M. Pioro-Ladrière, Nanotechnology **27**, 464003 (2016).

[33] M. Benito, X. Mi, J. M. Taylor, J. R. Petta, and G. Burkard, Phys. Rev. B **96**, 235434 (2017).

[34] A. M. Tyryshkin, S. Tojo, J. J. L. Morton, H. Riemann, N. V. Abrosimov, P. Becker, H.-J. Pohl, T. Schenkel, M. L. W. Thewalt, K. M. Itoh, and S. A. Lyon, Nat. Mater. **11**, 143 (2012).

[35] F. A. Zwanenburg, A. S. Dzurak, A. Morello, M. Y. Simmons, L. C. L. Hollenberg, G. Klimeck, S. Rogge, S. N. Coppersmith, and M. A. Eriksson, Rev. Mod. Phys. **85**, 961 (2013).

[36] K. D. Petersson, L. W. Mcfaul, M. D. Schroer, M. Jung, J. M. Taylor, A. A. Houck, and J. R. Petta, Nature **490**, 380 (2012).

[37] L. E. Bruhat, T. Cubaynes, J. J. Viennot, M. C. Dartiailh, M. M. Desjardins, A. Cottet, and T. Kontos, Phys. Rev. B **98**, 155313 (2018).

[38] A. Stockklauser, P. Scarlino, J. V. Koski, S. Gasparinetti, C. K. Andersen, C. Reichl, W. Wegscheider, T. Ihn, K. Ensslin, and A. Wallraff, Phys. Rev. X **7**, 011030 (2017).

[39] X. Mi, J. V. Cady, D. M. Zajac, P. W. Deelman, and J. R. Petta, Science **335**, 156 (2017).

[40] A. Cottet and T. Kontos, Phys. Rev. Lett. **105**, 160502 (2010).

[41] X. Hu, Y.-X. Liu, and F. Nori, Phys. Rev. B **86**, 035314 (2012).

[42] D. J. van Woerkom, P. Scarlino, J. H. Ungerer, C. Müller, J. V. Koski, A. J. Landig, C. Reichl, W. Wegscheider, T. Ihn, K. Ensslin, and A. Wallraff, Phys. Rev. X **8**, 041018 (2018).

[43] J. Majer, J. M. Chow, J. M. Gambetta, J. Koch, B. R. Johnson, J. A. Schreier, L. Frunzio, D. I. Schuster, A. A. Houck, A. Wallraff, A. Blais, M. H. Devoret, S. M. Girvin, and R. J. Schoelkopf, Nature **449**, 443 (2007).

[44] J. M. Fink, R. Bianchetti, M. Baur, M. Göppl, L. Steffen, S. Filipp, P. J. Leek, A. Blais, and A. Wallraff, Phys. Rev. Lett. **103**, 083601 (2009).

[45] A. Imamoglu, D. D. Awschalom, G. Burkard, D. P. DiVincenzo, D. Loss, M. Sherwin, and A. Small, Phys. Rev. Lett. **83**, 4204 (1999).

[46] G. Burkard and A. Imamoglu, Phys. Rev. B **74**, 041307 (2006).

[47] See Supplemental Material for details of the derivation of the Hamiltonian, the cavity damping and phonon relaxation terms, and for discussions of the average fidelity and charge noise.

[48] N. Schuch and J. Siewert, Phys. Rev. A **67**, 032301 (2003).

[49] M. Boissonneault, J. M. Gambetta, and A. Blais, Phys. Rev. A **79**, 013819 (2009).

[50] M. Horodecki, P. Horodecki, and R. Horodecki, Phys. Rev. A **60**, 1888 (1999).

[51] M. A. Nielsen, Phys. Lett. A **303**, 249 (2002).

[52] A. Gilchrist, N. K. Langford, and M. A. Nielsen, Phys. Rev. A **71**, 062310 (2005).

[53] A. G. White, A. Gilchrist, G. J. Pryde, J. L. O'Brien, M. J. Bremner, and N. K. Langford, J. Opt. Soc. Am. B **24**, 172 (2007).

[54] S. J. Elman, S. D. Bartlett, and A. C. Doherty, Phys. Rev. B **96**, 115407 (2017).

[55] N. Samkharadze, A. Bruno, P. Scarlino, G. Zheng, D. P. DiVincenzo, L. DiCarlo, and L. M. K. Vandersypen, Phys. Rev. Applied **5**, 044004 (2016).

[56] N. Maleeva, L. Grünhaupt, T. Klein, F. Levy-Bertrand, M. Dupre, O. Calvo, F. Valenti, P. Winkel, F. Friedrich, W. Wernsdorfer, A. V. Ustinov, H. Rotzinger, A. Monfardini, M. V. Fistul, and I. M. Pop, Nat. Commun. **9**, 3889 (2018).

[57] C. Leroux, L. C. G. Govia, and A. A. Clerk, Phys. Rev. Lett. **120**, 093602 (2018).

[58] C. Tahan and R. Joynt, Phys. Rev. B **89**, 075302 (2014).

[59] P. Arrangoiz-Arriola, E. A. Wollack, M. Pechal, J. D. Witmer, J. Hill, and A. H. Safavi-Naeini, Phys. Rev. X **8**, 031007 (2018).

[60] Y. J. Rosen, M. A. Horsley, S. E. Harrison, E. T. Holland, A. S. Chang, T. Bond, and J. L. DuBois, Appl. Phys. Lett. **114**, 202601 (2019).

[61] K. D. Petersson, J. R. Petta, H. Lu, and A. C. Gossard, Phys. Rev. Lett. **105**, 246804 (2010).

[62] X. Mi, S. Kohler, and J. R. Petta, Phys. Rev. B **98**, 161404 (2018).

[63] A. Blais, J. Gambetta, A. Wallraff, D. I. Schuster, S. M. Girvin, M. H. Devoret, and R. J. Schoelkopf, Phys. Rev. A **75**, 032329 (2007).

[64] G. Haack, F. Helmer, M. Mariantoni, F. Marquardt, and E. Solano, Phys. Rev. B **82**, 024514 (2010).

[65] V. Srinivasa, J. M. Taylor, and C. Tahan, Phys. Rev. B **94**, 205421 (2016).

[66] S. P. Harvey, C. G. L. Bøttcher, L. A. Orona, S. D. Bartlett, A. C. Doherty, and A. Yacoby, Phys. Rev. B **97**, 235409 (2018).

[67] S. Bosco and D. P. DiVincenzo, Phys. Rev. B **100**, 035416 (2019).

[68] A. Warren, E. Barnes, and S. E. Economou, arXiv:1902.05704.